Supporting information for:

Formation of Low Volatility Organic Compounds and Secondary Organic Aerosol from Isoprene Hydroxyhydroperoxide Low-NO Oxidation

Jordan E. Krechmer[†,‡], Matthew M. Coggon[§], Paola Massoli[∇], Tran B. Nguyen[§,□], John D. Crounse[□], Weiwei Hu[†,‡], Douglas A. Day[†,‡], Geoffrey S. Tyndall[■], Daven K. Henze[△], Jean C. Rivera-Rios[▲,%], John B. Nowak[∇], Joel R. Kimmel[∇,○], Roy L. Mauldin III[#], Harald Stark[†,‡,∇], John T. Jayne[∇], Mikko Sipilä[¶], Heikki Junninen[¶], Jason M. St. Clair[□,∫], Xuan Zhang[§], Philip A. Feiner[⊥], William H. Brune[⊥], Frank N. Keutsch[▲,%], Paul O. Wennberg[□], John H. Seinfeld[§,‖], Douglas R. Worsnop[∇], Jose L. Jimenez[†,‡,*], and Manjula R. Canagaratna[∇,*]

[†]Cooperative Institute for Research in Environmental Sciences (CIRES), Boulder, CO, 80309, USA
[‡]Department of Chemistry and Biochemistry, University of Colorado, Boulder, CO, 80309, USA
[§]Divisions of Chemistry and Chemical Engineering, California Institute of Technology, Pasadena, CA, 91125, USA
[∇]Center for Aerosol and Cloud Chemistry, Aerodyne Research, Billerica, MA, 01821, USA
[□]Division of Geological and Planetary Sciences, California Institute of Technology, Pasadena, CA, 91125, USA
[■]National Center for Atmospheric Research, Boulder, CO, 80301
[△]Department of Mechanical Engineering, University of Colorado, Boulder, CO, 80309, USA
[▲]Department of Chemistry, University of Wisconsin-Madison, Madison, WI, 53706, USA
[○]Tofwerk, AG, CH-3600, Thun, Switzerland
[#]Department of Atmospheric and Oceanic Sciences, University of Colorado, Boulder, CO 80309, USA
[¶]Department of Physics, University of Helsinki, 00014, Helsinki, Finland
[⊥]Department of Meteorology, Pennsylvania State University, University Park, PA, 16802, USA
[‖]Division of Engineering and Applied Science, California Institute of Technology, Pasadena, CA, 91125, USA

Correspondence to : M. R. Canagaratna <mrcana@aerodyne.com> and J.L. Jimenez, <jose.jimenez@colorado.edu>

This file includes:

Materials and Methods

NO_3^--CIMS Quantification.

The concentration of gas-phase species X measured by the NO_3^--CIMS is quantified as [1]:

$$[X]_{chamber} = \frac{S_{X \cdot NO_3^-}}{S_{NO_3^-} + S_{HNO_3NO_3^-} + S_{(HNO_3)_2NO_3^-}} \times C_x \quad [2]$$

where C_x is a compound-dependent calibration coefficient for a given temperature and pressure with units of molecules cm^{-3}, $S_{X \cdot NO_3^-}$ is the signal of the $X \cdot NO_3^-$ cluster, and the denominator is the sum of all reagent ions.

The calibration coefficient also includes signal loss due to diffusion-limited wall loss in the inlet tubing. This loss is included in the value of C as a multiplicative factor:[1]

$$C_{LVOC} = \frac{1}{f_{inlet}\, k_{ion}\, RT} \quad [3]$$

where f_{inlet} is the fraction of analyte that reaches the ionization source, and (1-f_{inlet}) is the fraction lost to the inlet walls via gaseous diffusion [2]. In this case, RT is the 200ms residence time of the analyte molecules in the ion/molecule reaction region, and represents the effect on the calibration coefficient from the amount of ion collisions in the charger. k_{ion} is the rate coefficient for ion formation from the analyte.

The value of f_{inlet} for the FIXCIT inlet was calculated to be ~7% using standard equations to calculate the loss of a species in a tube assuming laminar flow [2]. Inputs for this calculation include temperature (26C), pressure (98 kPa for a 252 m altitude in Pasadena, CA, USA), species diffusion coefficient for a model LVOC in air (~5 $x10^{-6}$ m^2 s^{-1}) estimated using the SPARC calculator [3,4], sample tube inner diameter (0.00476 m), tube length (2m), and air flow rate of $5x10^{-5}$ m^3 s^{-1} corresponding to the sample gas flow of 3 SLPM. This process assumes that these

species are of sufficiently low volatility that they are irreversibly lost to the walls (uptake coefficient of 1) and that there is no re-partitioning back to the gas-phase,[1] which is consistent with their behavior in the chamber as discussed elsewhere in this work. There is some uncertainty from this assumption, which is probably comparable with the uncertainty arising from the ion-molecule reaction rates. We also note that non-condensing species may also not be lost to the walls of the tubing. Thus we may overestimate the concentration of non-condensing species, but this is of no consequence to our analyses since these species do not contribute to the novel aerosol formation pathway discussed here.

The value of k_{ion} was estimated experimentally from laboratory calibrations. Low-volatility oxidized species were introduced into the NO_3^--CIMS via a heated diffusion cell and quantified via conversion to CO_2 by a heated platinum catalyst. The CO_2 was then measured using a LI-840A CO_2 analyzer (LI-COR).[5] The FIXCIT inlet was used in the calibrations to maintain the same f_{inlet} values. Malonic acid ($C_3H_4O_4$) was the most sensitive organic compound tested and was used as the primary LVOC calibrant since it is thought to cluster at rates close to the collision limit [6]. The calibration factor calculated from Equation 3 using the malonic acid k_{ion} measurements and FIXCIT f_{inlet} of 7% is $C = 7.9 \times 10^{10}$ molec. cm^{-3}. We apply the experimentally obtained value of $C = 7.9\times10^{10}$ molec. cm^{-3} for malonic acid to all of the measured LVOC because it has the highest sensitivity and therefore provides a lower bound on the LVOC concentrations. For comparison, the calibration factor calculated for sulfuric acid, which charges at a collision limited rate in the nitrate source,[7] is within 11 % (C_{LVOC} of 7.0×10^{10} molec. cm^{-3}, using k_{ion} value of 5×10^{9} molec. cm^{-3} from previous work[8] and our calculated value of $f_{inlet} = 0.07$) of the calibration factor calculated for malonic acid in this work. The assumption that all the detected LVOC species cluster with the reagent ion at or close to the

collision limit is dependent on the LVOC having highly oxidized functional group contributions (e.g., hydroxyl and hydroperoxy) resulting in large dipole moments and polarizabilities, which is consistent with their measured elemental compositions and condensing behavior (discussed below).[9]

To track system stability and repeatability, a signal calibration was performed periodically, before or after experiments, by flowing a steady concentration of diethylene glycol (DEG) for several minutes, which was quantified using a catalytic converter and CO_2 analyzer following the method of Veres et al.[5] The instrument showed excellent stability and repeatability.

Fragmentation and clustering are not thought to play a significant role in the detection of LVOC. First, previous work has shown that formation of water clusters is not a preferred pathway in the ionization process.[10] Second, the NO_3^--CIMS efficiently measures oxidized dimers and trimers.[11] No dimers or trimers were detected and thus it is very unlikely that the LVOC are fragments of larger molecules.

CIMS bulk elemental analysis and uncertainty. The following equation was used to estimate the bulk elemental oxygen to carbon ratio (O:C) contribution to the aerosol phase from the 14 LVOC detected by the NO_3^--CIMS:

$$\frac{O}{C} = \frac{\sum_{n=1}^{14}[LVOC]_n O_n}{\sum_{m=1}^{14}[LVOC]_m C_m} \qquad [4]$$

where O_n and C_m are the number of oxygen or carbon atoms, respectively, for a selected LVOC and $[LVOC]_n$ is the fractional contribution of each LVOC to the total condensed LVOC signal. The $[LVOC]_n$ were assigned based on the percent mixing ratios observed lost to the aerosol-phase (as shown in Figure 2b). A similar equation was used for the elemental hydrogen to elemental carbon ratio, H:C:

$$\frac{H}{C} = \frac{\sum_{n=1}^{14}[LVOC]_n H_n}{\sum_{m=1}^{14}[LVOC]_m C_m} \quad [5]$$

where H_n and C_m are the number of hydrogen and carbon atoms, respectively for a selected LVOC.

A Monte Carlo simulation was performed to estimate the uncertainty of the O:C and H:C bulk elemental ratios for gas-phase organics measured by the NO_3^--CIMS. We assumed a relative uncertainty in the calibration factors between different LVOCs of 100%. In each run of the Monte Carlo method, the concentration of each LVOC was scaled with a random sensitivity consistent with the estimated uncertainty, and then used to calculate the weighted average O:C and H:C ratios. The simulation was run 100,000 times (Figure S13) and the value of the 2σ deviation for each bulk elemental ratio was used as the uncertainty.

Kinetic Box Model Details. Hydroxyl radical (OH) concentrations in the chamber were estimated using the observed decay rate of ISOPOOH and its published reaction rate with OH.[12,13]

The aerosol uptake rate was modeled using the following equation:

$$k_{uptake} = \frac{1}{4}\bar{c}A\gamma \quad [1]$$

where $\bar{c}$ is the mean speed of LVOC molecules in the gas-phase, γ is the uptake coefficient, and A is the aerosol surface area.[14] Because the particles are small (< 50 nm), the correction for the transition regime is small and can be neglected.[14] Aerosol surface area was not measured for this experiment, so this quantity was estimated from measurements of a non-seeded, low-NO isoprene+OH oxidation experiment carried out on a different date with similar conditions in the same chamber. The total aerosol surface area time series in the model was reduced using the

surface-area-to-mass ratio ($\frac{2}{3}$ power relationship) to account for the lower amount OA observed in this FIXCIT experiment. A loss rate for gas-phase species to the walls (k_{wall}) is also included in the model. As a first guess we utilize a value of 0.002 s^{-1}, which was taken from previous modeling of the Caltech chamber,[15] and this value is optimized with the model. It is important to note that it is not possible to experimentally determine wall uptake coefficients larger than ~6×10^{-6} from chamber experiments.[16] Wall loss rates for gas-phase species determined by the model were used to correct all SOA formation yields presented in this work.

The loss rate for organic aerosol to the chamber walls (2.5×10^{-4} s^{-1}) was constrained from the observed AMS SOA signal decay after the end of the photochemistry, which agrees with typical values for the particle sizes expected in this experiment for the Caltech chamber.[17] While the particle loss rate has a dependency on particle size, we estimate the range of particles observed in the AMS to be of a narrow size range from 50 to 150 nm. Particles smaller than 50 nm are not detected by the AMS and the particles are likely not larger than 150 nm because there is so little mass in this experiment. This would result in a variation of the particle wall loss rate of the order of a factor of 1.5 at most, for any realistic size distribution.[18] This is similar or smaller than the uncertainty in other parameters.

NO_3^--CIMS observations were used to constrain the values of k_{wall}, γ_{SOA}, and the yield of LVOC from their formation reactions.

Because the structures of LVOC are relatively similar to IEPOX (and do not contain double bonded carbon atoms), the loss rate for LVOC via reaction with OH is assumed to be similar to those of IEPOX with OH (0.8 -1.5 $\times10^{-11}$ cm^3 $molec^{-1}$ s^{-1}, isomer-dependent).[19] The integrated reaction rates are a few percent of the LVOC loss rates via aerosol formation or deposition to the chamber walls and are therefore not included in the model.

Some of the LVOC may contain hydroperoxide groups that are susceptible to photolysis. We can estimate their photolysis lifetime as 4.1 days using the chamber light intensity and spectrum, and the absorption cross section of hydroxymethylhydroperoxide (HHMP, $HOCH_2OOH$) as a surrogate species of similar functionality.[20] This results in a decay of 2% over the course of our experiment. Since the functional group composition of each LVOC is not precisely known and the photolyzed fraction of hydroperoxides is very small, photolysis is neglected in our model.

Uncertainty estimation for the model parameters, k_{wall}, γ_{SOA}, and the reaction yield (Y). Estimation of the model parameters (k_{wall}, γ_{SOA}, and Y) that provide the best fit to experimental data was treated as a nonlinear regression problem. The optimization was based on minimizing the sum of the squares of the residuals (χ^2) between the model and observations. The optimization was performed in two ways: automatically, using the FuncFit function in Igor Prof 6, and manually. In the manual mode the model was run 10,000 times, stepping through different values of k_{wall}, γ_{SOA}, and Y. For each model result, the χ^2 of the model and measured traces were evaluated.

The uncertainties in the fitted model parameters ($\mathbf{m}_{L2} = [k_{wall}, \gamma_{SOA}, Y]^T$) were evaluated using the statistics of nonlinear regression.[21] We obtain 95% confidence limits on the model parameters by:[21]

$$\sigma = 1.96\ \mathrm{diag}(\mathrm{Cov}(\mathbf{m}_{L2}))^{1/2} \qquad [6]$$

We estimate the covariance matrix (inverse Hessian) for the fitted model parameters as:[21]

$$\mathrm{Cov}(\mathbf{m}_{L2}) \approx s^2 \left(\mathbf{J}(\mathbf{m}_{L2})^T \mathbf{J}(\mathbf{m}_{L2})\right)^{-1} \qquad [7]$$

where Cov($\mathbf{m}_{L2}$) is the covariance matrix for a the model results linearized about $\mathbf{m}_{L2}$, s is the measurement standard deviation, and $\mathbf{J}(\mathbf{m}_{L2})$ is the Jacobian matrix ($d\mathbf{r}/d\mathbf{m}$) of the residual vector $\mathbf{r}$, calculated about the least-squares solution $\mathbf{m}_{L2}$ using finite differences.

PMF analysis of ambient AMS data during SOAS. We obtained a time series of ambient ISOPOOH-SOA in the SOAS dataset by using the constrained positive matrix factorization (PMF) method as implemented in the multilinear engine (ME-2) software. In this analysis one of the factors extracted from the ambient organic data was constrained to have a mass spectrum that is similar to the FIXCIT ISOPOOH-SOA AMS spectrum. The theoretical principles of PMF ME-2 are described by Paatero.[22] ME-2 was run via the SoFi interface, v.4.6.[23] For the ME-2 setup, a range of a-values between 0 – 0.3 (fully constrained to partially constrained) were tested. We found clear and consistent time series of ISOPOOH-SOA in these different cases. We could not extract an ISOPOOH-SOA component in the free-PMF source apportionment, likely due to the low abundance of this factor (~2%) in the total OA being below the estimated detection limit of PMF (~5%).[24] Other sources of OA, including isoprene epoxydiols-derived SOA (IEPOX-SOA), monoterpene-derived SOA, and biomass burning OA (BBOA), are also resolved out concurrent with ISOPOOH-SOA, consistent with published PMF results for this study and site from another group.[25]

Discussion of the Potential Impact of the Impurities in the ISOPOOH Standard

As discussed in the main paper several additional OVOCs were introduced in the chamber together with ISOPOOH, at a molar rate of 7% to ISOPOOH. For several reasons, we believe that it is improbable that the majority of LVOC and resulting SOA produced in this

experiment arose from the impurities rather than the 4,3-ISOPOOH itself. First, the yield of SOA from all species in this experiment is ~4.2%. The LVOC that condense are not the contaminants themselves, since they are only observed when the UV lights are turned on and photochemical oxidation is active. Therefore, the contaminants would have to have SOA yields of ~60% in order to explain all the SOA formation. There are no known 4 or 5 carbon organic species that have an SOA yield of ~60%, and it is extremely unlikely that most of the diverse molecules comprising the impurities could have such high SOA yields. With a more typical SOA yield comparable to that of ISOPOOH, the contribution of the impurities to be observed SOA would be minor.

The likely major oxidation product of the tentatively-identified 2-carbonyl-3-methyl-3-butane-1-ol impurity (Fig. S2) has an estimated vapor pressure (Table S3) 100 times too large to be condensing quickly at an OA level of 0.2 μg m^{-3}, as observed during this experiment. Even taking into account the uncertainty of the vapor pressure estimation method of a factor of 10 [26], this discrepancy is still too large by x10. Also, its amount is 25 times too small to explain the amount of $C_5H_{10}O_5$ observed in this experiment. Therefore we do not expect a significant contribution from this impurity to the observed condensing $C_5H_{10}O_5$ species.

The $C_5H_{12}O_5$ LVOC signal also is a possible product of from the tentatively-identified 3-methyl-3-butane-1,2-diol impurity (Fig. S2). The molar yield of a $C_5H_{12}O_5$ product could be ~60% from the impurity, based on structure-reactivity relationships.[27] Since this impurity is present at a level of ~1% of ISOPOOH and is estimated to react with OH at a similar rate, we can derive an upper limit yield of 0.6% as the molar ratio of the $C_5H_{12}O_5$ arising from the contaminant. Thus the SOA yield may be lower by that amount, assuming the identification, mechanisms, and estimated volatility of the products of this impurity are correct. We note that if

that is the case, this 4,3-alkene-diol would represent a unique case of a C5 species with a phenomenal 60% SOA yield via condensation at OA levels below 1 μg m^{-3}, which is at least an order-of-magnitude larger than has been determined from any C5 species including isoprene and ISOPOOH, to our knowledge. In any case the reduction of the SOA yield arising from this potential correction is small compared to other uncertainties in the experimental and modeling system.

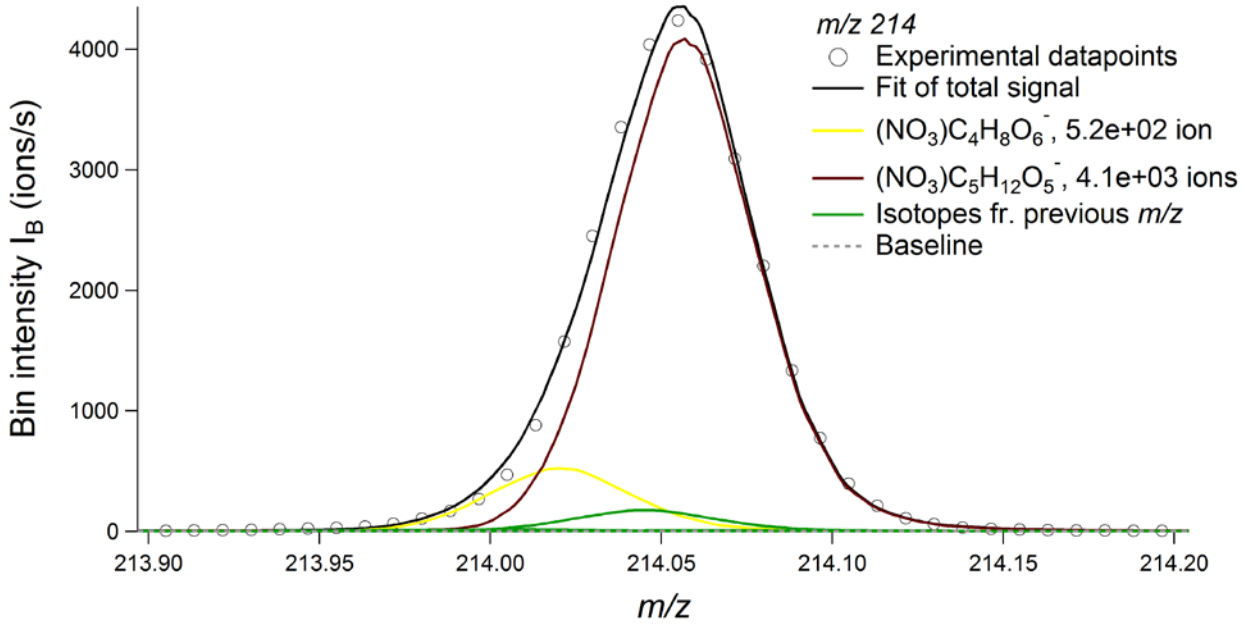

Figure S1. The high resolution mass spectrum peak fit for *m/z* 214, which is dominated by the $C_5H_{12}O_5$ LVOC.

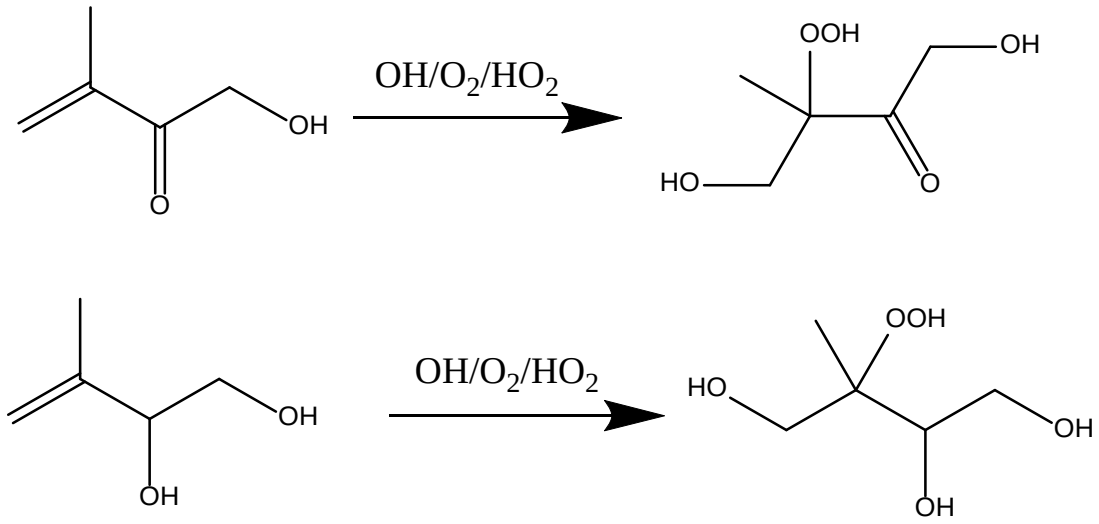

Figure S2. A mechanism showing the tentatively identified impurities of the 4,3-ISOPOOH standard (on the left) and their possible low-NO OH·-initiated reaction products on the right. Only products of addition to the double bond are shown, although it is estimated that 30% of the reaction proceeds via hydrogen abstraction for the lower structure.

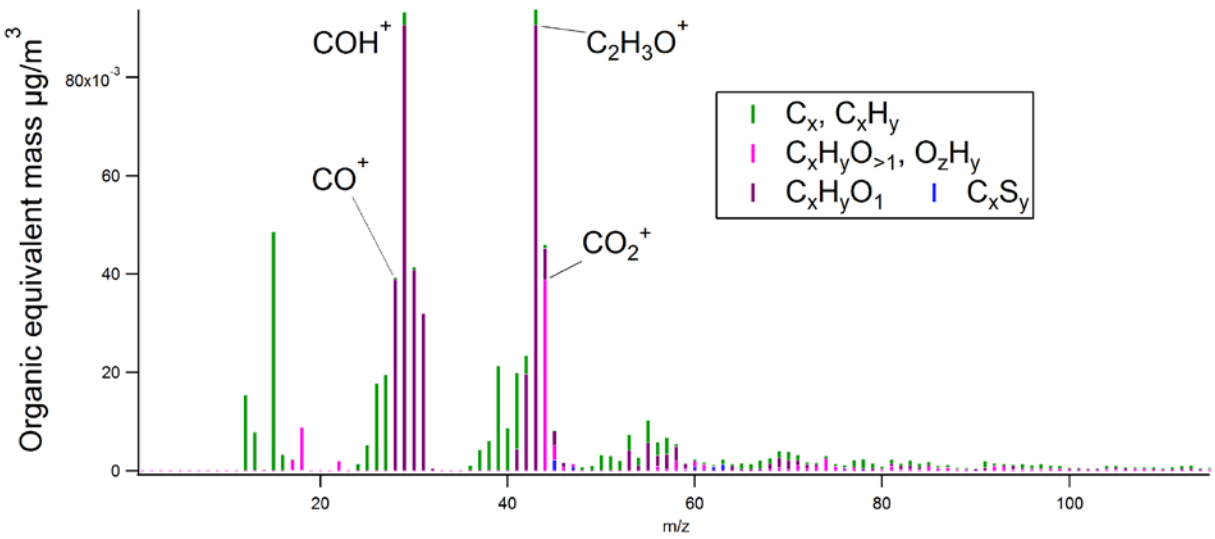

Figure S3. AMS spectrum at the point of peak gas-phase LVOC condensation (SOA concentration 0.61 µg m^{-3}). The signals at *m/z* 29 and 43 are similar by coincidence.

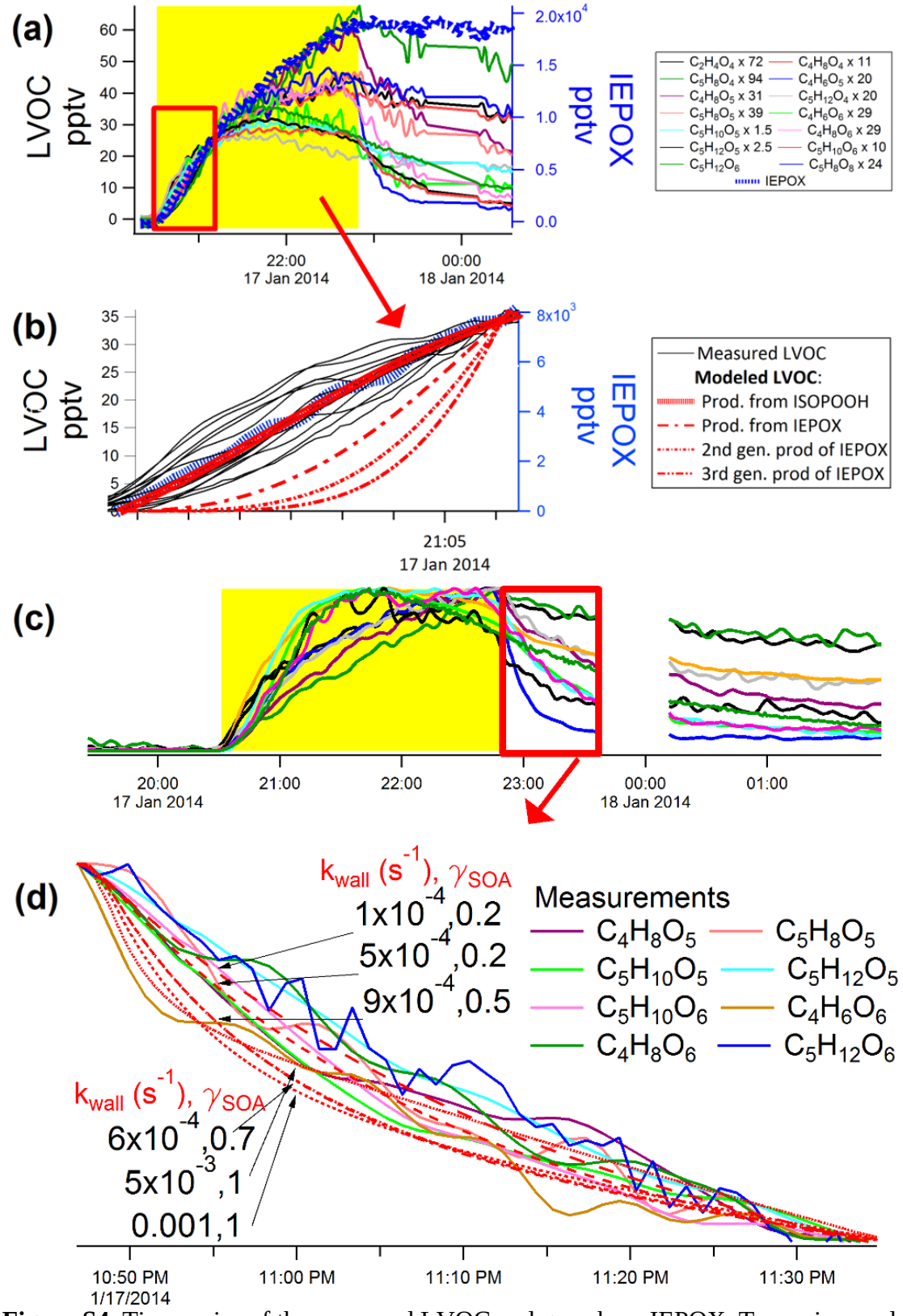

Figure S4. Time series of the measured LVOC and gas-phase IEPOX. Traces in panels **(a)** and **(b)** are scaled to overlap at the time in the experiment in which SOA was first detected, and the

point when UV lights are turned off in panels **(c)** and **(d)**. Panel **b** is a close-up of a. Panel **d** depicts the highlighted region in panel **c**, with the starting concentration scaled to one arbitrary point and the concentration observed at 23:35 scaled to zero. Model results for a range of wall loss rates and aerosol uptake coefficients are also shown. This has been modeled with the parameters also used in Fig. 4. For clarity, not all LVOC are shown in panel **d**. In panels **a** and **b** IEPOX has been binomially smoothed (5 points) and in panel **d** the LVOC have been binomially smoothed (5 points).

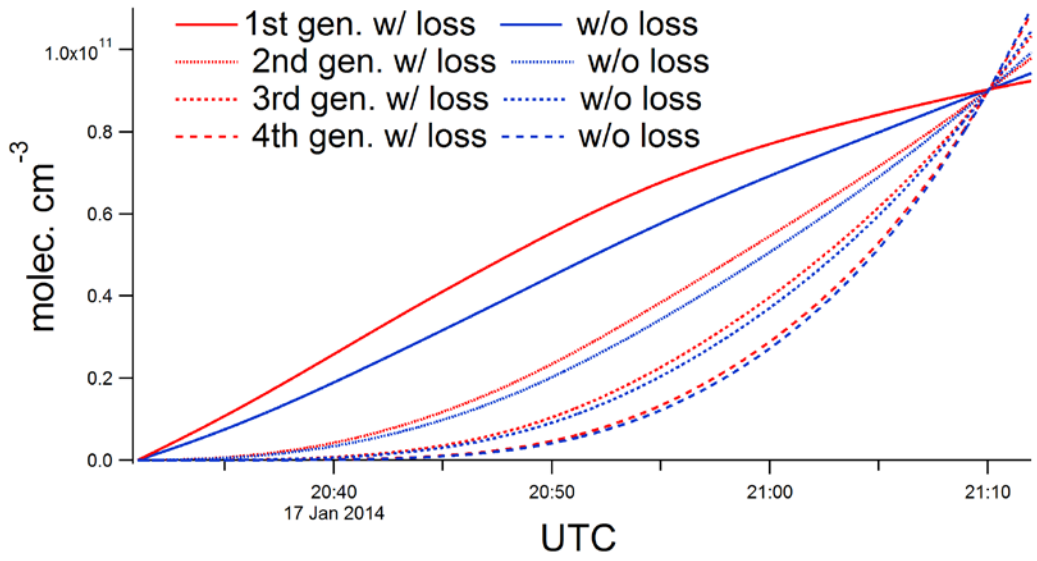

Figure S5. Time evolution of the products from different generations of oxidation calculated with the kinetic model with and without wall losses. The contribution of wall losses during the initial period shown is small. The traces are all scaled to the value of the largest trace at 21:10 UTC.

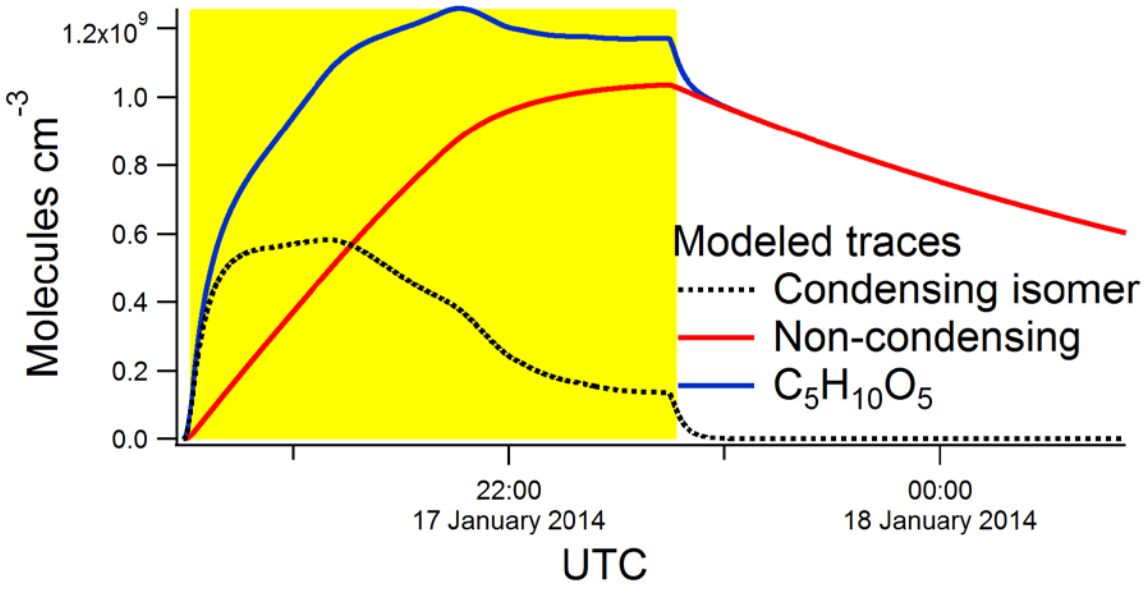

Figure S6. Time series for the two modeled isomers that comprise the $C_5H_{10}O_5$ modeled trace. The isomer that condenses is of low-volatility and is rapidly lost to the walls and aerosol as soon as the lights are turned off. The non-condensing isomer is slowly lost to the walls and accounts for the large amount of sum $C_5H_{10}O_5$ remaining at the end of the experiment. Note that the non-condensing isomer may be lost to the inlet less efficiently than the condensing isomer, and thus may have an overestimated concentration, but this is of no consequence for the SOA modeling.

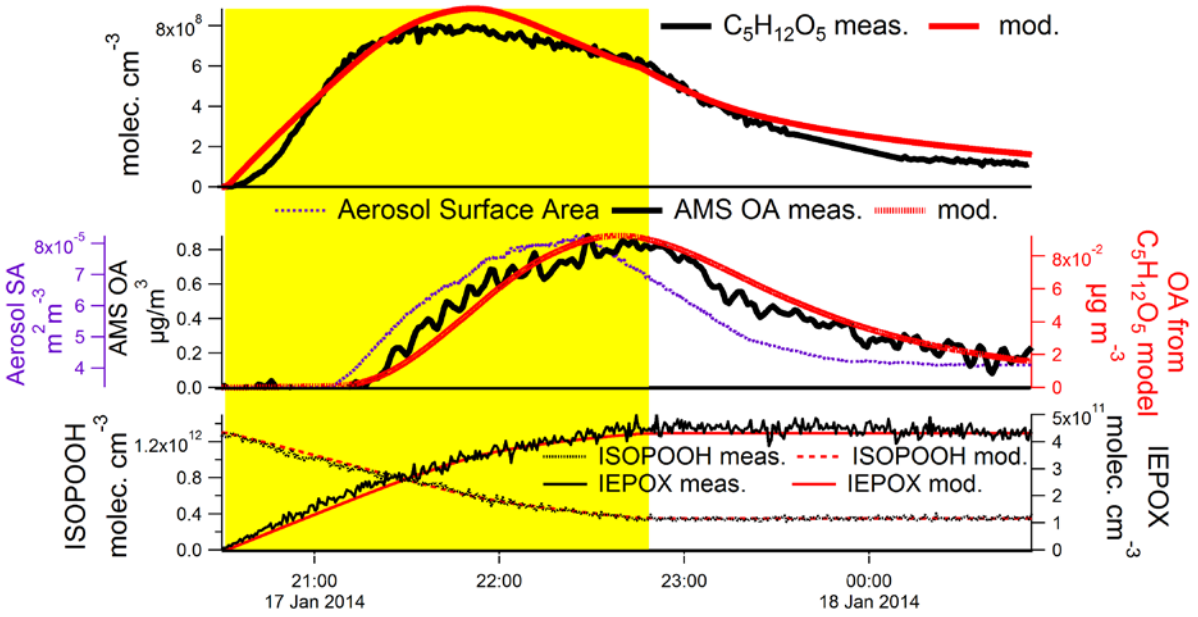

Figure S7. Time series of measured (red) and modeled (black) gas and aerosol concentrations for $C_5H_{12}O_5$. The LVOC was fit with one modeled species with optimized values of $\gamma_{SOA} = 0.2$, $k_{wall} = 1 \times 10^{-4}$, and an ISOPOOH + OH reaction rate branching ratio of 0.4%. The model SOA (middle, right axis) gives the approximate fractional contribution of $C_5H_{12}O_5$ and the surface area has been binomially smoothed across 10 points.

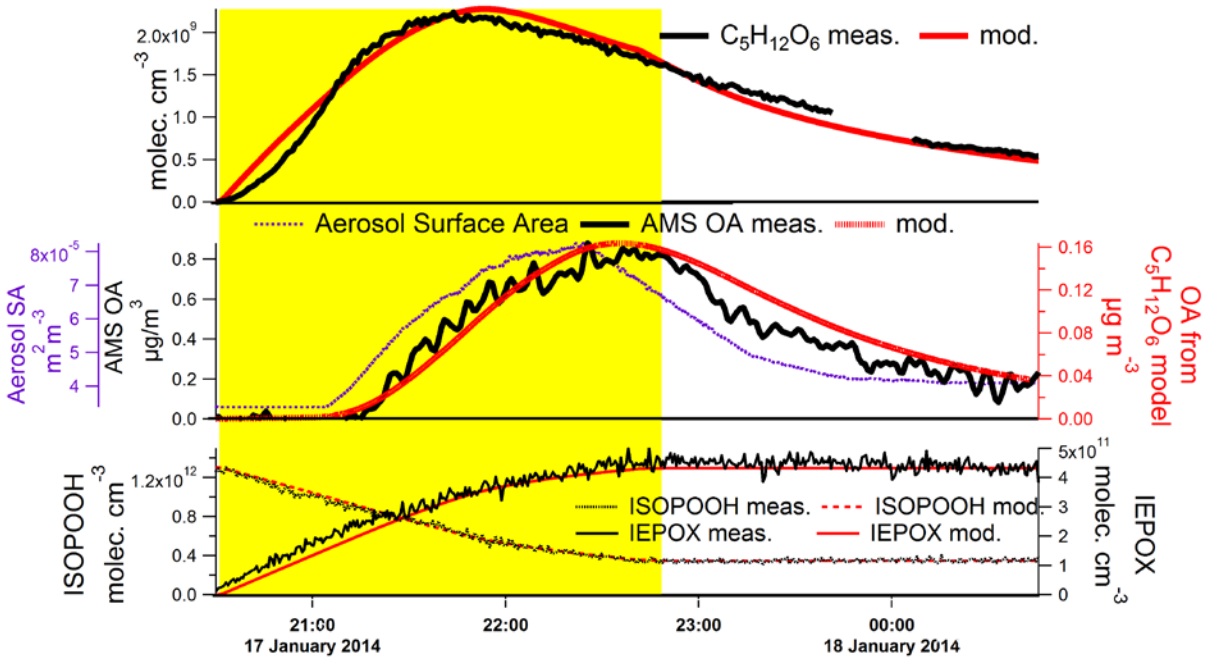

Figure S8. Model time series for C5H12O6. The model was run with $C_5H_{12}O_6$ as a first-generation product of ISOPOOH oxidation. This LVOC was fit with one modeled species using values of $\gamma_{SOA} = 0.1$ and $k_{wall} = 1.5\times10^{-4}$ s^{-1} and an ISOPOOH + OH reaction rate branching ratio of 1.0%. The model SOA (middle, right axis) gives the approximate fractional contribution of $C_5H_{12}O_6$ and the surface area has been binomially smoothed across 10 points.

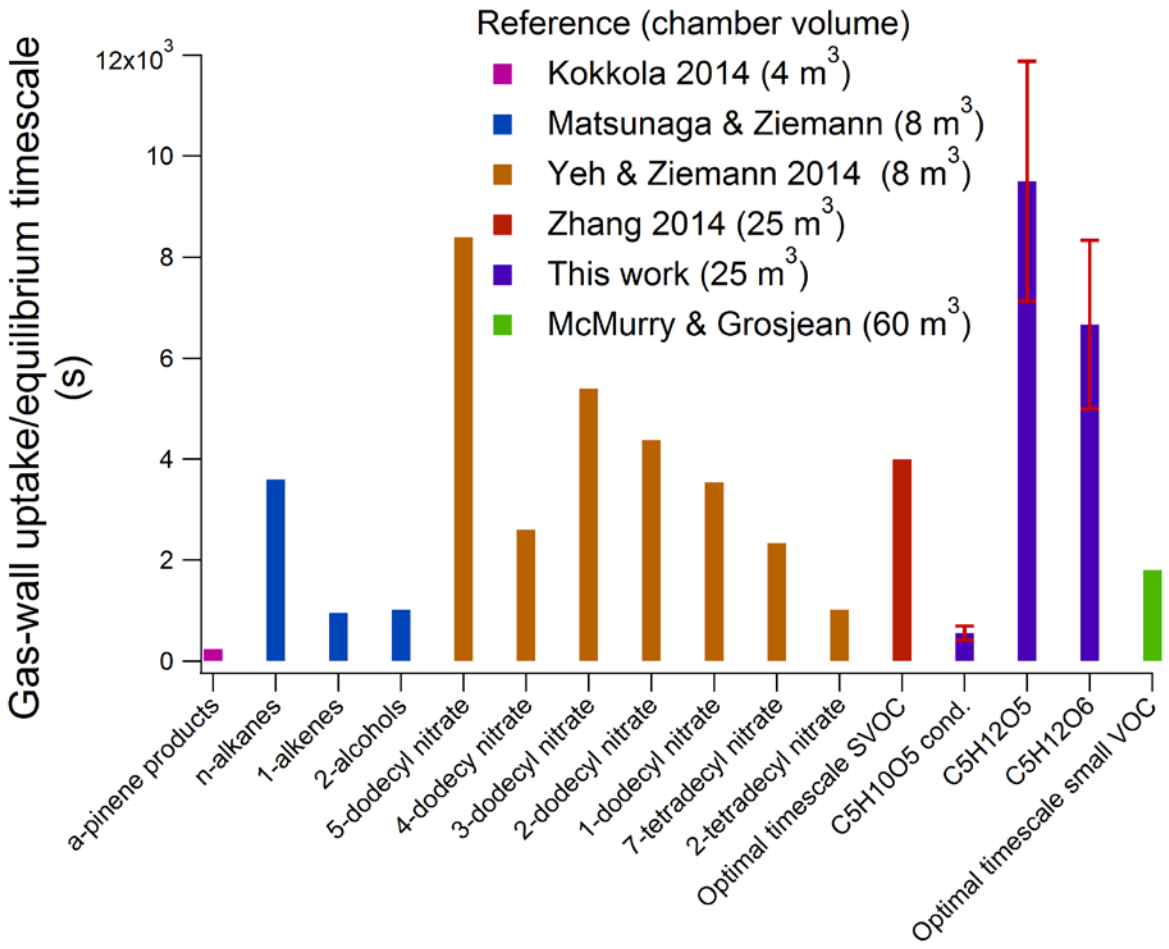

Figure S9. Gas-wall equilibrium timescales from gas-phase species in this work compared to values presented in previous works. Previous values are taken from Zhang et al., Yeh and Ziemann [28], McMurry and Grosjean[16], Matsunaga and Ziemann [29], and Kokkola et al. [30].

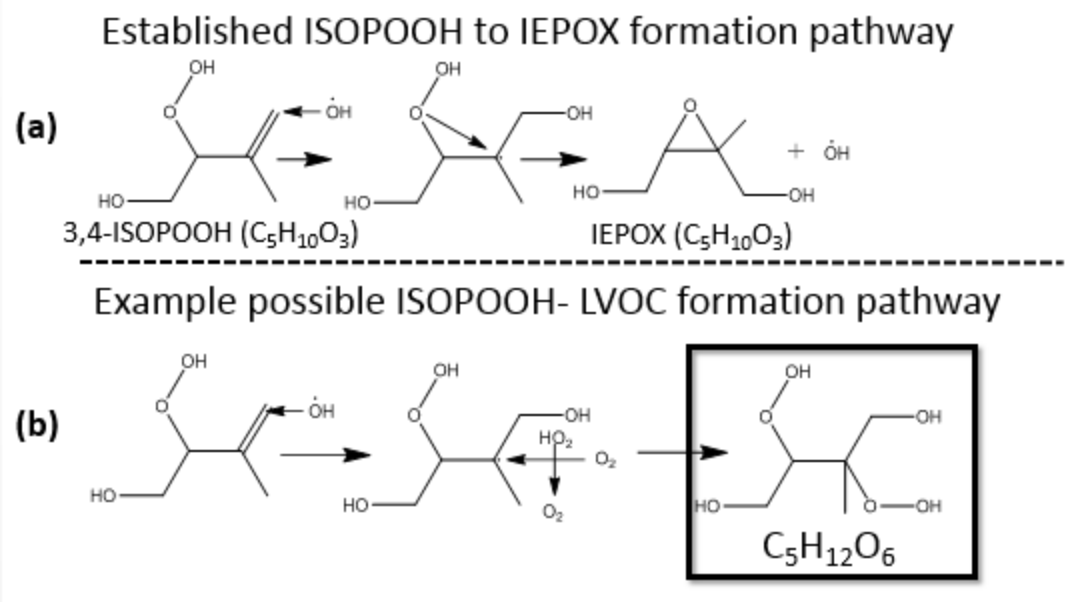

Figure S10. Possible formation mechanism for one of the observed LVOC: $C_5H_{12}O_6$, as originally proposed in Paulot et al.[12] A species consistent with the elemental composition of the species in the square was detected in this study by the NO_3^--CIMS. Reaction **b** proceeds via addition of the hydroxyl radical one side of the double bond in ISOPOOH, producing the same intermediate as for IEPOX. However, then addition of O_2 occurs at the adjacent tertiary carbon followed by reaction with HO_2 that transfers a hydrogen atom, forming a hydroperoxy group. The established IEPOX formation mechanism **(a)** is shown above for comparison.

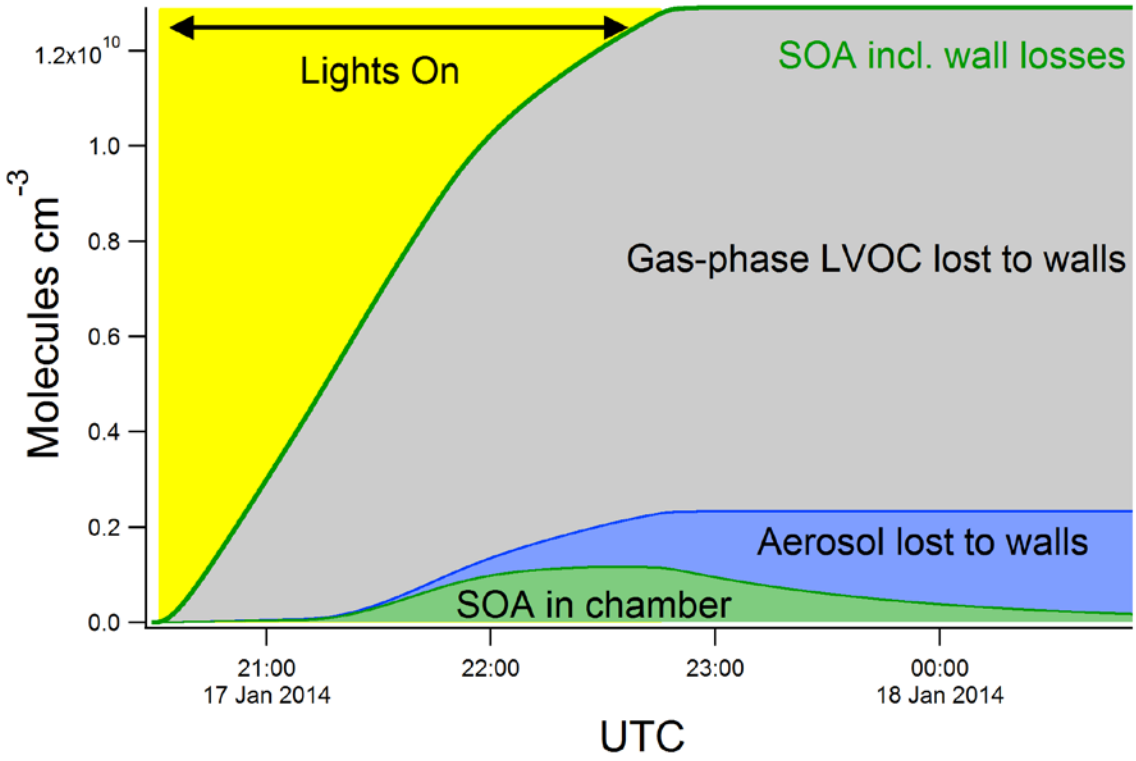

Figure S11. Model results for runs with and without sinks to the chamber walls for $C_5H_{10}O_5$. The difference between the two models is used to calculate the increase in SOA yield as it incorporates the amount of gas-phase material that could have formed SOA, if losses to the walls had not been active. The traces are stacked on top of one another.

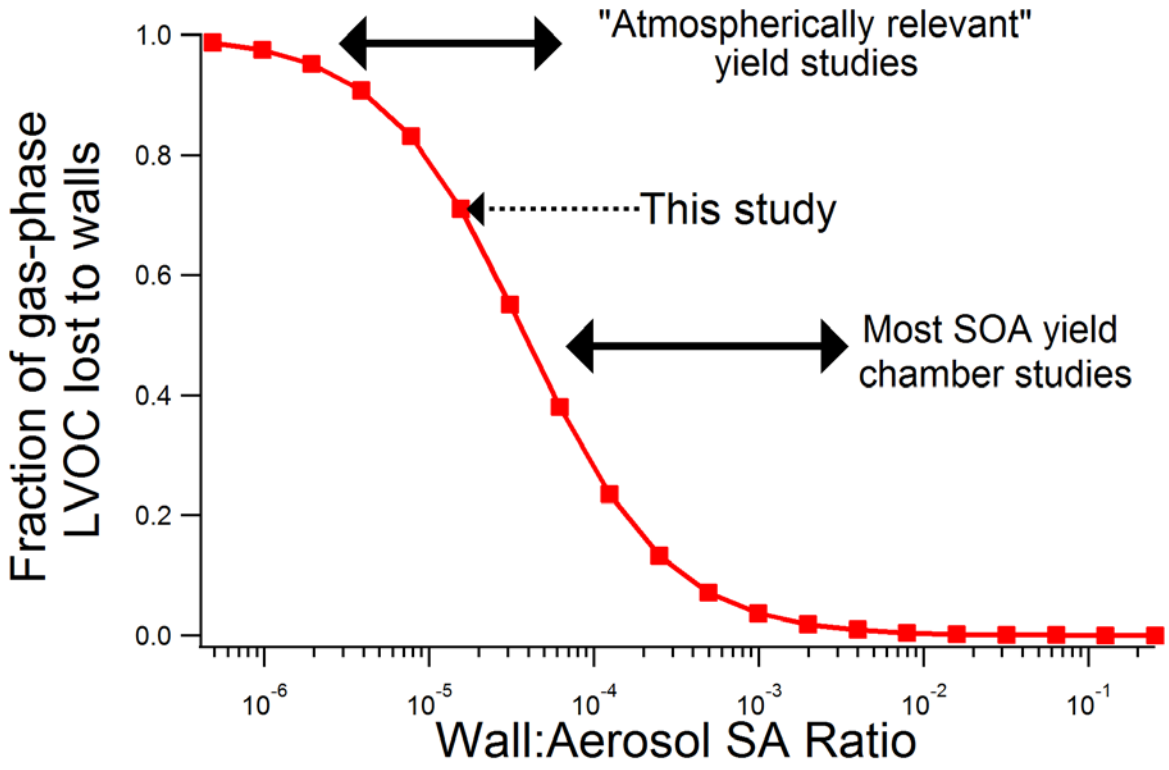

Figure S12. The fraction of gas-phase LVOC lost to the chamber walls versus the Wall:Aerosol surface area ratio, calculated using the kinetic box model and assuming a constant aerosol surface area for each case, for simplicity. Note that this figure assumes irreversible condensation with the SOA uptake coefficient γ_{SOA} = 1.0 determined for $C_5H_{10}O_5$ in this study.

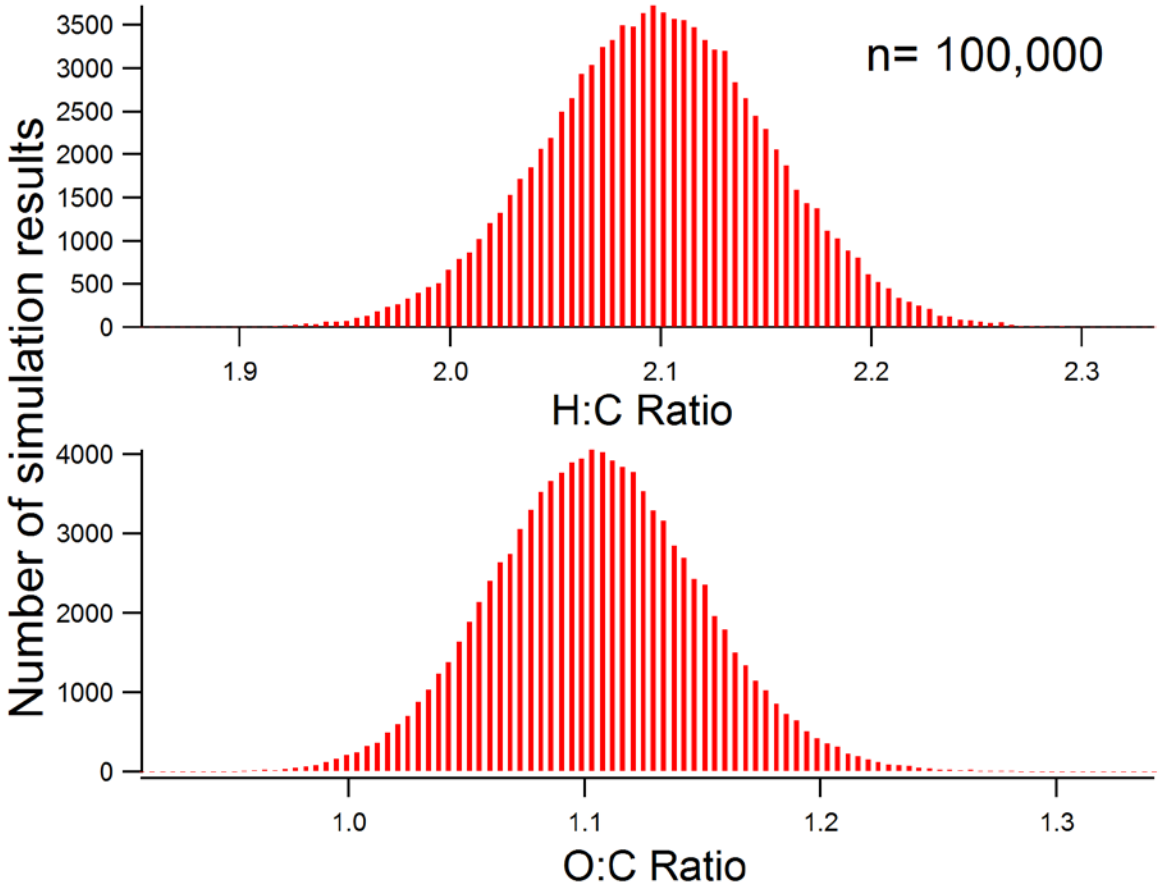

Figure S13. Histograms showing the results of the Monte Carlo simulation to determine the uncertainty of the CIMS elemental bulk ratios. The Monte Carlo simulation was run 100,000 times.

Elemental Formula	Ion Exact Mass	Species Mass [Da]	H:C	O:C	OS_C
$C_2H_4O_4$	153.9993	92.0110	2.00	2.00	2.00
$C_4H_8O_4$	182.0306	120.0423	2.00	1.00	0.00
$C_5H_8O_4$	194.0306	132.0423	1.60	0.80	0.00
$C_4H_6O_5$	196.0099	134.0215	1.50	1.25	1.00
$C_4H_8O_5$	198.0255	136.0372	2.00	1.25	0.50
$C_5H_{12}O_4$	198.0619	136.0736	2.40	0.80	-0.80
$C_5H_8O_5$	210.0250	148.0372	1.60	1.00	0.40
$C_4H_6O_6$	212.0048	150.0164	1.50	1.50	1.50
$C_5H_{10}O_5$	212.0412	150.0528	2.00	1.00	0.00
$C_4H_8O_6$	214.0205	152.0321	2.00	1.50	1.00
$C_5H_{12}O_5$	214.0568	152.0685	2.40	1.00	-0.40
$C_5H_{10}O_6$	228.0356	166.0477	2.00	1.20	0.40
$C_5H_{12}O_6$	230.0518	168.0634	2.4	1.2	0
$C_5H_8O_8$	258.00979	196.02196	1.6	1.6	1.6

Table S1. Elemental formulas, exact masses, and elemental properties of the 14 ions observed condensing into the aerosol-phase.

Species or condition	**Initial value**
ISOPOOH	1.29 x 10^{12} molecules cm^{-3}
Temperature	25 °C
RH	< 5%

Reaction	**Rate Coefficient at 25 °C (cm^3 $molecule^{-1}$ s^{-1} unless noted otherwise)**	**Reference**
ISOPOOH + OH→	7.9×10^{-11}	Paulot et al. 2009, 2012 [12,13], Xie et al. 2013 [31]
→ IEPOX + OH	88%	
→ $C_5H_{10}O_5^c$	2.5%	This work
→$C_5H_{10}O_5^{nc}$	0.6%	This work
→Other Products	8.9%	
IEPOX + OH→Other Products	1.5×10^{-11}	Bates et al. 2014 [19]
OA→Wall	2.5×10^{-4} s^{-1}	Cocker et al. 2001 [17]
$C_5H_{10}O_5^c$ →Wall	3.0×10^{-3} s^{-1}	This work
$C_5H_{10}O_5^c$ → SOA	2.2×10^{-3} at peak 1.4×10^{-5} mean ($\gamma = 1.0$)	Seinfeld & Pandis [14] This work
$C_5H_{10}O_5^{nc}$ → Wall	7×10^{-5} s^{-1}	This work
$C_5H_{10}O_5^{nc}$ → SOA	0 s^{-1}	

Table S2. Kinetic box model initial conditions, reactions, and rate coefficients to reproduce the observed time-dependent behavior of $C_5H_{10}O_5$. The non-condensing isomer of $C_5H_{10}O_5$ is denoted with a “nc” superscript, the condensing isomer with a “c” superscript.

Table S3. List of possible functional group compositions for all elemental formulas of observed LVOC, along with their estimated saturation concentrations (C^*) estimated with the SIMPOL model.[32] Contributions are listed from: "N_c", the number of carbon atoms; "C=O", ketones and aldehydes; "OH," hydroxyl groups; "COOH," carboxylic acids; "OOH," hydroperoxyl groups; "CO(O)OH," peroxy acids; and "C=C," carbon-carbon double bonds. The impact of C^* of aldehydes and ketones are only slightly different, so they were grouped together here for simplicity.

Elemental Formula	C* (μg m^{-3})	Nc	-C=O	-OH	-C(O)OH	-OOH	-C(O)OOH	-C=C	Fraction Lost
C2H4O4	5.79E+05	2		1			1		0.42
C2H4O4	2.05E+04	2			1	1			
C4H8O4	4.88E+01	4		2	1				0.32
C4H8O4	1.25E+02	4	1	3					
C4H8O4	3.53E+03	4			1	1			
C4H8O4	9.08E+03	4	1	1		1			
C4H8O4	2.68E+04	4				2		1	
C4H8O4	9.96E+04	4		1			1		
C5H8O4	1.55E+01	5		2	1			1	0.01
C5H8O4	3.98E+01	5	1	3				1	
C5H8O4	1.48E+02	5			2				
C5H8O4	3.80E+02	5	1	1	1				
C5H8O4	9.76E+02	5	2	2					
C5H8O4	1.12E+03	5			1	1		1	
C5H8O4	2.88E+03	5	1	1		1		1	
C5H8O4	3.16E+04	5		1			1	1	
C5H8O4	7.07E+04	5	2			1			
C5H8O4	7.75E+05	5	1				1		
C4H6O5	2.43E+00	4		1	2				0.29
C4H6O5	6.25E+00	4	1	2	1				
C4H6O5	4.74E+01	4	1	2		1		1	
C4H6O5	4.53E+02	4	1		1	1			

C4H6O5	1.16E+03	4	2	1		1			
C4H6O5	3.44E+03	4	1			2		1	
C4H6O5	4.97E+03	4			1		1		
C4H6O5	1.28E+04	4	1	1			1		
C4H6O5	3.77E+04	4				1	1	1	
C4H8O5	3.25E-01	4		3	1				0.21
C4H8O5	2.36E+01	4		1	1	1			
C4H8O5	6.06E+01	4	1	2		1			
C4H8O5	6.64E+02	4		2			1		
C4H8O5	4.39E+03	4	1			2			
C4H8O5	4.81E+04	4				1	1		
C5H12O4	2.65E+00	5		4					0.86
C5H12O4	1.92E+02	5		2		1			
C5H12O4	1.39E+04	5				2			
C5H8O5	1.29E-01	5		3	1				0.17
C5H8O5	3.30E-01	5	1	4					
C5H8O5	9.75E-01	5		1	2				
C5H8O5	2.51E+00	5	1	2	1				
C5H8O5	6.44E+00	5	2	3					
C5H8O5	7.40E+00	5		1	1	1		1	
C5H8O5	2.39E+01	5	1	2		1			
C5H8O5	1.82E+02	5	1		1	1			
C5H8O5	2.09E+02	5		2			1	1	
C5H8O5	4.67E+02	5	2	1		1			
C5H8O5	1.73E+03	5	1			2			
C5H8O5	4.07E+03	5	1	1		1			
C5H8O5	5.12E+03	5	1	1			1		
C5H8O5	1.51E+04	5				1	1	1	
C4H6O6	1.60E-02	4		2	2				0.4
C4H6O6	6.68E-01	4					2		
C4H6O6	1.16E+00	4			2	1			
C4H6O6	2.98E+00	4	1	1	1	1			
C4H6O6	2.26E+01	4	1	1		2		1	

C4H6O6	3.27E+01	4		1	1		1		
C4H6O6	8.41E+01	4	1	2			1		
C4H6O6	5.56E+02	4	2			2			
C4H6O6	6.09E+03	4	1			1	1		
C4H6O6	2.21E+05	4	2			1			
C5H10O5	1.30E-01	5		3	1				0.69
C5H10O5	2.43E+01	5	1	2		1			
C5H10O5	7.16E+01	5		1		2		1	
C5H10O5	1.76E+03	5	1			2			
C5H10O5	3.35E-01	5	1	4					
C4H8O6	3.99E-01	4	1	3		1			0.3
C4H8O6	2.89E+01	4	1	1		2			
C4H8O6	3.17E+02	4		1		1	1		
C5H12O5	1.26E+00	5		3		1			0.48
C5H12O5	9.15E+01	5		1		2			
C5H12O5	9.15E+01	5		1		2			
C5H10O6	6.15E-02	5		2	1	1			0.9
C5H10O6	1.44E-01	5		3	1				
C5H10O6	1.58E-01	5	1	3		1			
C5H10O6	4.67E-01	5		2		2		1	
C5H10O6	3.38E+01	5				3		1	
C5H10O6	1.26E+02	5		1		1	1		
C5H12O6	5.95E-01	5		2		2			0.14
C5H12O6	4.31E+01	5				3			
C5H8O8	1.10E-05	5		2			2		0.27
C5H8O8	1.91E-05	5		2	2	1			
C5H8O8	1.45E-04	5		2	1	2		1	
C5H8O8	7.96E-04	5				1	2		
C5H8O8	1.38E-03	5			2	2			
C5H8O8	3.56E-03	5	1	1	1	2			

C5H8O8	4.08E-03	5		3		1	1	1	
C5H8O8	1.05E-02	5			1	3		1	
C5H8O8	1.00E-01	5	1	2		1	1		
C5H8O8	2.96E-01	5		1		2	1	1	
C5H8O8	6.62E-01	5	2			3			
C5H8O8	6.94E-01	5		2		1	1	1	
C5H8O8	1.63E+00	5		3			1	1	
C5H8O8	7.26E+00	5	1			2	1		

Supp. Info. References:

(1) Ehn, M.; Thornton, J. A.; Kleist, E.; Sipilä, M.; Junninen, H.; Pullinen, I.; Springer, M.; Rubach, F.; Tillmann, R.; Lee, B.; et al. A large source of low-volatility secondary organic aerosol. *Nature* **2014**, *506*, 476–479.

(2) Brockmann, J. E. Sampling and transport of aerosols. In *Aerosol measurement: Principles, Techniques, and Applications*; Wiley-Interscience: New York, 2001; pp. 143–195.

(3) Hilal, S. H.; Karickhoff, S. W.; Carreira, L. A. Prediction of the Vapor Pressure Boiling Point, Heat of Vaporization and Diffusion Coefficient of Organic Compounds. *QSAR Comb. Sci.* **2003**, *22*, 565–574.

(4) Hilal, S. H.; Saravanaraj, A. N.; Whiteside, T.; Carreira, L. A. Calculating physical properties of organic compounds for environmental modeling from molecular structure. *J. Comput. Aided. Mol. Des.* **2007**, *21*, 693–708.

(5) Veres, P.; Gilman, J. B.; Roberts, J. M.; Kuster, W. C.; Warneke, C.; Burling, I. R.; de Gouw, J. Development and validation of a portable gas phase standard generation and calibration system for volatile organic compounds. *Atmos. Meas. Tech.* **2010**, *3*, 683–691.

(6) Ehn, M.; Junninen, H.; Petäjä, T.; Kurtén, T.; Kerminen, V.-M.; Schobesberger, S.; Manninen, H. E.; Ortega, I. K.; Vehkamäki, H.; Kulmala, M.; et al. Composition and temporal behavior of ambient ions in the boreal forest. *Atmos. Chem. Phys.* **2010**, *10*, 8513–8530.

(7) Viggiano, A.; Perry, R.; Albritton, D.; Ferguson, E.; Fehsenfeld, F. C. Stratospheric negative-ion reaction rates with H2SO4. *J. Geophys. Res. Ocean.* **1982**, *87*, 7340–7342.

(8) Mauldin, R.; Tanner, D.; Eisele, F. Measurements of OH during PEM-Tropics A. *J. Geophys. Res.* **1999**, *104*, 5817–5827.

(9) Garden, A. L.; Paulot, F.; Crounse, J. D.; Maxwell-Cameron, I. J.; Wennberg, P. O.; Kjaergaard, H. G. Calculation of conformationally weighted dipole moments useful in ion–molecule collision rate estimates. *Chem. Phys. Lett.* **2009**, *474*, 45–50.

(10) Rissanen, M. P.; Kurtén, T.; Sipilä, M.; Thornton, J. A.; Kangasluoma, J.; Sarnela, N.; Junninen, H.; Jørgensen, S.; Schallhart, S.; Kajos, M. K.; et al. The formation of highly oxidized multifunctional products in the ozonolysis of cyclohexene. *J. Am. Chem. Soc.* **2014**, *136*, 15596–15606.

(11) Ehn, M.; Kleist, E.; Junninen, H.; Petäjä, T.; Lönn, G.; Schobesberger, S.; Dal Maso, M.; Trimborn, a.; Kulmala, M.; Worsnop, D. R.; et al. Gas phase formation of extremely oxidized pinene reaction products in chamber and ambient air. *Atmos. Chem. Phys.* **2012**, *12*, 5113–5127.

(12) Paulot, F.; Crounse, J. D.; Kjaergaard, H. G.; Kürten, A.; St Clair, J. M.; Seinfeld, J. H.; Wennberg, P. O. Unexpected epoxide formation in the gas-phase photooxidation of isoprene. *Science* **2009**, *325*, 730–733.

(13) Paulot, F.; Henze, D. K.; Wennberg, P. O. Impact of the isoprene photochemical cascade on tropical ozone. *Atmos. Chem. Phys.* **2012**, *12*, 1307–1325.

(14) Seinfeld, J. H.; Pandis, S. N. *Atmospheric chemistry and physics: from air pollution to climate change*; 2nd ed.; John Wiley & Sons, Inc.: Hoboken, New Jersey, USA, 2006; Vol. 2nd.

(15) Zhang, X.; Cappa, C. D.; Jathar, S. H.; McVay, R. C.; Ensberg, J. J.; Kleeman, M. J.; Seinfeld, J. H. Influence of vapor wall loss in laboratory chambers on yields of secondary organic aerosol. *Proc. Natl. Acad. Sci. U.S.A.* **2014**, *111*, 5802–5807.

(16) McMurry, P. H.; Grosjean, D. Gas and aerosol wall losses in Teflon film smog chambers. *Environ. Sci. Technol.* **1985**, *19*, 1176–1182.

(17) Cocker, D. R.; Flagan, R. C.; Seinfeld, J. H. State-of-the-art chamber facility for studying atmospheric aerosol chemistry. *Environ. Sci. Technol.* **2001**, *35*, 2594–2601.

(18) Crump, J. G.; Seinfeld, J. H. Turbulent deposition and gravitational sedimentation of an aerosol in a vessel of arbitrary shape. *J. Aerosol Sci.* **1981**, *12*, 405–415.

(19) Bates, K. H.; Crounse, J. D.; St Clair, J. M.; Bennett, N. B.; Nguyen, T. B.; Seinfeld, J. H.; Stoltz, B. M.; Wennberg, P. O. Gas phase production and loss of isoprene epoxydiols. *J. Phys. Chem. A* **2014**, *118*, 1237–1246.

(20) Keller-Rudek, H.; Moortgat, G. K.; Sander, R.; Sörensen, R. The MPI-Mainz UV/VIS spectral atlas of gaseous molecules of atmospheric interest. *Earth Syst. Sci. Data* **2013**, *5*, 365–373.

(21) Aster, R. C.; Thurber, C. H.; Borchers, B. *Parameter Estimation and Inverse Problems*; International geophysics series; Elsevier Academic Press: Boston, 2005.

(22) Paatero, P. *End user's guide to multilinear engine applications*; University of Helsinki: Helsinki, Finland, 2007.

(23) Canonaco, F.; Crippa, M.; Slowik, J. G.; Baltensperger, U.; Prévôt, a. S. H. SoFi, an IGOR-based interface for the efficient use of the generalized multilinear engine (ME-2) for the source apportionment: ME-2 application to aerosol mass spectrometer data. *Atmos. Meas. Tech.* **2013**, *6*, 3649–3661.

(24) Ulbrich, I. M.; Canagaratna, M. R.; Zhang, Q.; Worsnop, D. R.; Jimenez, J. L. Interpretation of organic components from Positive Matrix Factorization of aerosol mass spectrometric data. *Atmos. Chem. Phys.* **2009**, *9*, 2891–2918.

(25) Xu, L.; Guo, H.; Boyd, C. M.; Klein, M.; Bougiatioti, A.; Cerully, K. M.; Hite, J. R.; Isaacman-VanWertz, G.; Kreisberg, N. M.; Knote, C.; et al. Effects of anthropogenic emissions on aerosol formation from isoprene and monoterpenes in the southeastern United States. *Proc. Natl. Acad. Sci. U.S.A.* **2015**, *112*, 37–42.

(26) Barley, M. H.; McFiggans, G. The critical assessment of vapour pressure estimation methods for use in modelling the formation of atmospheric organic aerosol. *Atmos. Chem. Phys.* **2010**, *10*, 749–767.

(27) Ziemann, P. J.; Atkinson, R. Kinetics, products, and mechanisms of secondary organic aerosol formation. *Chem. Soc. Rev.* **2012**, *41*, 6582–6605.

(28) Yeh, G. K.; Ziemann, P. J. Identification and yields of 1,4-hydroxynitrates formed from the reactions of C8-C16 n-alkanes with OH radicals in the presence of NO(x). *J. Phys. Chem. A* **2014**, *118*, 8797–8806.

(29) Matsunaga, A.; Ziemann, P. J. Gas-Wall Partitioning of Organic Compounds in a Teflon Film Chamber and Potential Effects on Reaction Product and Aerosol Yield Measurements. *Aerosol Sci. Technol.* **2010**, *44*, 881–892.

(30) Kokkola, H.; Yli-Pirila, P.; Vesterinen, M.; Korhonen, H.; Keskinen, H.; Romakkaniemi, S.; Hao, L.; Kortelainen, A.; Joutsensaari, J.; Worsnop, D. R.; et al. The role of low volatile organics on secondary organic aerosol formation. *Atmos. Chem. Phys.* **2014**, *14*, 1689–1700.

(31) Xie, Y.; Paulot, F.; Carter, W. P. L.; Nolte, C. G.; Luecken, D. J.; Hutzell, W. T.; Wennberg, P. O.; Cohen, R. C.; Pinder, R. W. Understanding the impact of recent advances in isoprene photooxidation on simulations of regional air quality supplementary information. *Atmos. Chem. Phys.* **2013**, *13*, 8439–8455.

(32) Pankow, J. F.; Asher, W. E. SIMPOL.1: a simple group contribution method for predicting vapor pressures and enthalpies of vaporization of multifunctional organic compounds. *Atmos. Chem. Phys.* **2008**, *8*, 2773–2796.